Electronic structure of $CeAuAl_3$ using density functional theory

André Deyerling[1⋆], Marc A. Wilde[1] and Christian Pfleiderer[1,2,3]

1 Physik Department, Technische Universität München, D-85748 Garching, Germany
2 MCQST, Technische Universität München, D-85748 Garching, Germany
3 Centre for Quantum Engineering (ZQE), Technische Universität München, D-85748 Garching, Germany
* andre.deyerling@tum.de

August 14, 2022

International Conference on Strongly Correlated Electron Systems (SCES 2022)
Amsterdam, 24-29 July 2022
doi:10.21468/SciPostPhysProc.?

Abstract

We studied the magnetic properties and electronic structure of $CeAuAl_3$ using density functional theory. This compound shows a large Sommerfeld coefficient, $\gamma > 200\,\frac{\mathrm{mJ}}{\mathrm{molK^2}}$, a Kondo temperature, $T_k = 4\,\mathrm{K}$ [1] and antiferromagnetic order below $T_N = 1.1\,\mathrm{K}$ [2]. We calculated the magnetic groundstate of $CeAuAl_3$ and the magnetic anisotropy energies. Treating the 4f-electrons as localized with DFT+U we obtain a good match with the magnetic properties observed experimentally. We also report salient features of the electronic structure of $CeAuAl_3$, including features of the Fermi surface and associated quantum oscillatory spectra, when the 4f-electrons are treated either as localized or itinerant.

1 Introduction

Cerium based compounds attract significant interest due to strong competing energy scales that lead to heavy fermion behavior, magnetic order, superconductivity and magneto-elastic coupling. For the family of $CeTAl_3$ compounds (T=Ag, Au, Cu, Pd, Pt) different forms of magnetic order [3] and coupling between crystal field states and phonons have attracted great interest in recent years [4,5]. The physical properties are tightly linked to the 4f-electrons and their interaction with the conduction electrons. In order to obtain a better understanding of the hybridization between the f- and conduction electrons a detailed study of the electronic structure of these compounds is required. An important concept when discussing the electronic structure is the relation between localized and itinerant 4f-electrons and the observation of a small or large Fermi surface according to the Luttinger theorem [6,7]. The small or large Fermi surface are often found in different parts of the field-temperature-pressure phase diagram [8–10]. Relatively unexplored so far is the electronic structure of the series of $CeTAl_3$ compounds both theoretically or experimentally. We present calculations of the magnetic properties and electronic structure of $CeAuAl_3$ as obtained using density functional theory.

2 Computational methods

For our calculations we used the full potential APW+lo method as implemented in WIEN2k [11] and Elk [12]. WIEN2k was used to calculate the properties for collinear magnetic order in $CeAuAl_3$ whereas Elk was used for the helical non collinear magnetic structures. For the latter the generalized Bloch theorem was used which allows to calculate magnetic structures with long wavelength modulations within the chemical unit cell [13]. The itinerant 4f-electron picture was addressed using DFT calculations whereas the propreties assuming a localized 4f-electron were calculated using DFT+U. For the Hubbard correction (DFT+U) the implementation of Liechtenstein et al. [14] was used in the fully localized limit and J is set to 0. In DFT+U calculations multiple local minima corresponding to different occupations of the 4f-states are expected [15]. To determine the global minimum multiple local minima were explored by starting with a fixed 4f-density matrix and relaxing it in a second calculation. The lowest energy solution was taken as the global minimum. For the electronic structure and magnetic properties presented in the following, the room temperature experimental lattice constants were used [16]. No significant changes were observed when using optimized lattice constants. Further technical information on the calculations may be found in Appendix A.

3 Results

Conflicting terminology is often used when discussing the character of 4f-electrons in heavy fermion systems. In the following we distinguish the following notions: localized magnetism, localized 4f-electron, and itinerant 4f-electron. Localized magnetism means that the magnetic properties of a 4f-electron compound are well described without major contributions from a hybridization of the f-electrons with the conduction electrons such as the Kondo effect. With localized 4f-electrons and itinerant 4f-electrons we refer to the large and small Fermi surfaces in the sense of Luttingers theorem. Localized magnetism is always found for localized 4f-electrons but not vice versa. In the following sections we will show that the experimental findings and our own ab initio calculations are consistent with the picture of localized magnetism. We will then give predictions for the large and the small Fermi surface in this compound and comment where in the magnetic phase diagram one or the other may be expected.

3.1 Physical properties

The physical properties of $CeAuAl_3$ relevant to the character of the 4f-electron and the applicability of density functional theory may be summarized as follows. $CeAuAl_3$ forms in a tetragonal crystal structure with space group I4mm, which lacks inversion symmetry [16]. Fermi liquid behavior [1] in combination with heavy fermion masses ($\gamma > 200\,\frac{\mathrm{mJ}}{\mathrm{molK^2}}$) [1, 2], have been reported for low temperatures. The Kondo temperature is estimated to be around 4 K based on the specific heat [1,2], and around 30 K based on the thermo-power [17]. Applying a magnetic field strongly suppresses the Sommerfeld coefficient γ [2]. Around $B = 2\,\mathrm{T}$ the Sommerfeld coefficient amounts to $1/4$ of the zero field value. It should be noted, however, that there is a large discrepancy between γ reported by Paschen et al. [1] and Adroja et al. [2]. This may be attributed to difficulties in extracting γ due to the presence of an anomaly associated with the magnetic transition. A magnetic phase transition from a paramagnetic to an antiferromagnetic state occurs at $T_N = 1.1\,\mathrm{K}$ [1, 2, 17, 18]. The ordering vector k of this structure is $(0, 0, 0.52)\,2\pi/\mathrm{c}$ and the ordered moment at the Ce site is $1.05\,\mu_\mathrm{B}$ [2]. A large magnetic anisotropy has been reported where the magnetic easy axis is parallel to the a-axis and the hard magnetic axis is parallel to the c-axis [18]. Such a large magnetic anisotropy suggests a preva-

lent influence of the crystal electric fields being associated with a localized 4f-electron as the origin of the magnetic properties. Also, the Curie-Weiss moment is consistent with the value expected for a free Ce^{3+} ion [1, 18]. In inelastic neutron scattering magneto-elastic coupling between the first excited crystal field state and acoustic phonons has been reported [5]. In this study, the hybridization strength between the conduction- and the 4f-electrons was found to be very low for temperatures between 4K and 300K as compared to the localized 4f-electrons in $CeAl_2$ [19]. Thus, the experimental findings already suggest where to expect a large Fermi surface due to Kondo coupling (heavy fermion masses) and where to expect a small Fermi surface (light masses).

3.2 Ab initio results

The presentation of the ab initio results is organized in three parts starting with the structural properties, followed by the magnetic properties, and the electronic structure last. First insights into the relevance of the localized electron picture may be inferred from the structural properties of $CeAuAl_3$. Structure optimization of the lattice constants and atomic positions was performed for different input parameters including the treatment of localized and itinerant 4f-electrons. Key results are summarized in table 1. The optimized crystal structures for localized 4f-electrons (table 1 lines 3-6) match experiment very well at low temperatures (table 1 line 2). The differences in volume are below 2.2% and the difference in c/a below 1.3%. Comparing the localized description (table 1 lines 3-6) with the itinerant description (table 1 line 7), the localized description displays a better agreement between the calculated crystal structures and experiment as compared to the case of itinerant 4f-electrons. GGA+U (PBE, PBEsol) captures the unit cell volume V and the size of the lattice constants a and c better than LDA+U. However, the ratio of the lattice constants is best reproduced for LDA+U in good agreement with experiment.

	V (Å^3)	a (Å)	c (Å)	c/a
Experiment (293.15 K) [16]	204.026	4.337	10.850	2.502
Experiment (0.30 K) [2]	200.603	4.310	10.796	2.505
PBE (non-magnetic) U=4 eV	203.620	4.314	10.940	2.536
PBEsol (spin polarized) U=4 eV	201.753	4.310	10.861	2.520
PBEsol (non-magnetic) U=4 eV	196.436	4.260	10.824	2.536
LDA (spin polarized) U=4 eV	196.333	4.274	10.750	2.494
LDA (spin polarized) U=0	193.022	4.262	10.629	2.627

Table 1: Crystal structure of $CeAuAl_3$ as obtained from structure optimization using DFT. Unit cell volume V, lattice constants a and c and their ratio c/a are compared to the high and low temperature structural parameters as observed in experiment. Good agreement is observed for the treatment of localized 4f-electrons (LDA/PBE/PBEsol+U) and the low temperature crystal structure at $T = 0.3$ K.

The results on the magnetic groundstate properties show on the whole that localized magnetism accounts well for the properties of $CeAuAl_3$. The magnetic properties were calculated using the LDA functional as the GGA functionals in combination with DFT+U show a large suppression of the orbital moment. This observation was earlier reported for fcc Cerium and appears to be a general characteristic of the GGA functionals [20]. We addressed the helical magnetic order of $CeAuAl_3$ and the spin polarized state corresponding to large magnetic fields. The latter also provides information on the magnetic anisotropy. Changing the direction of the

collinear spin arrangement in the spin polarized state is similar to changing the direction of the magnetic field in experiment.

U (eV)	4f-electron	$E_{100} - E_{001}$ (meV)
0	(Itinerant)	-2.11
2	(Localized)	-5.74
4	(Localized)	-6.72

Table 2: Dependence of magnetic anisotropy energy on the degree of localization of the 4f-electron of $CeAuAl_3$.

Direction $\vec{m}$	Itinerant	Localized	Experiment
[100]	$0.10\,\mu_B$	$0.87\,\mu_B$	$1.20\,\mu_B$
[001]	$0.03\,\mu_B$	$0.50\,\mu_B$	$0.42\,\mu_B$

Table 3: Total magnetic moment at the Ce site of $CeAuAl_3$ for the a- and c-axis. The reference values from experiment are the spontaneous magnetic moment for magnetic fields along the a- and the c-axis when extrapolating B to zero [18].

The magnetic anisotropy energy (table 2) and the size of the magnetic moments (table 3) observed for the localized 4f-electron correspond to an easy axis along the a-axis and a hard axis along the c-axis consistent with experiment. The size of the total magnetic moments parallel to the a- and c-axis is comparable to the spontaneous magnetic moment for magnetic fields along the a- and c-axis when extrapolating B to zero [18]. The total magnetic moment is dominated by the orbital contribution.

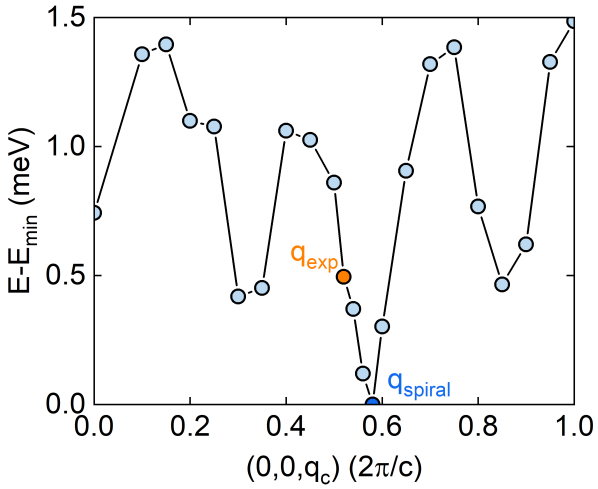

Figure 1: Total energy of $CeAuAl_3$ when varying the magnetic ordering vector q along the c-direction. The calculated minimum for a spin spiral at q_{spiral} is close to the value observed experimentally, q_{exp}.

Using the generalized Bloch theorem we calculated the magnetic properties for the helical magnetic order. We find that only the localized 4f-electron picture (LDA+U) can stabilize a magnetic structure in agreement with experiment. Itinerant 4f-electrons lead to non-magnetic

solutions. The energy differences between different magnetic ordering vectors for the localized 4f-electron are small which makes it necessary to use very fine k-grids and tight convergence criteria. Preliminary results are shown in figure 1. The small differences are somewhat expected as the magnetic phase transition is observed at very low temperatures. We conclude that the localized magnetism (DFT+U) captures the groundstate magnetic properties of $CeAuAl_3$ quite well.

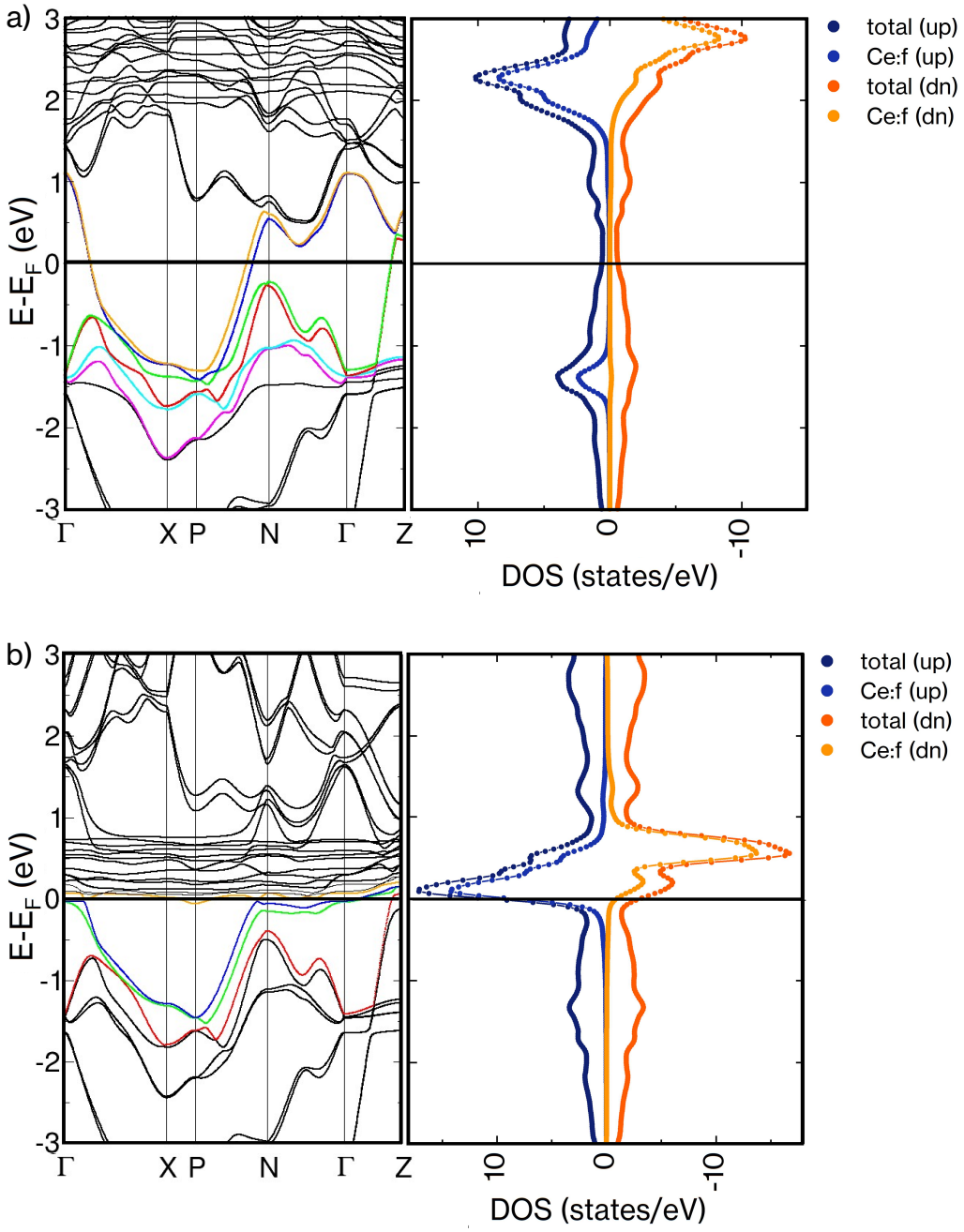

Figure 2: Band structure and density of states of $CeAuAl_3$: a) Results assuming localized 4f-electron (LDA+U+SOC with U=4 eV), b) Results assuming itinerant 4f-electron (LDA+SOC). The assignment of colors to the bands which cross the Fermi level corresponds to the assignment used for the Fermi surfaces shown in figure 3.

Regarding the electronic structure of $CeAuAl_3$, to the best of our knowledge, no studies of

the bandstructure using, e.g., quantum oscillations or ARPES have been reported. As pointed out above, localized and itinerant 4f-electrons may be expected in different parts of the magnetic phase diagram. The results of the DFT calculations predict an electronic structure of $CeAuAl_3$ with a localized or an itinerant 4f-electron. Further, we show that the itinerant and localized cases are easily distinguishable by their bandstructures and Fermi surfaces which are depicted in figures 2 and 3, respectively. For the localized 4f-electrons there are 6 bands crossing the Fermi level. The 4f-electrons have a binding energy of 1.5 eV and do not contribute to the Fermi surface. On the other hand for itinerant 4f-electrons, the band dispersion of the conduction electrons differs around the Fermi energy. Only 4 bands contribute to the Fermi surface. For ease of comparison between these two settings we use the same color code when labeling the bands. Due to the formation of flat 4f-electron bands a large contribution to the density of states by the 4f-electrons is observed around E_F. A direct comparison of the density of states obtained in DFT to the large Sommerfeld coefficients observed in experiments [1,2] is not possible. Such a large coefficient would require a more elaborate account of the interaction of the f-electrons with the conduction electrons beyond DFT and the scope of this study. In contrast, the topology of the Fermi surface is usually well-accounted in DFT [21,22].

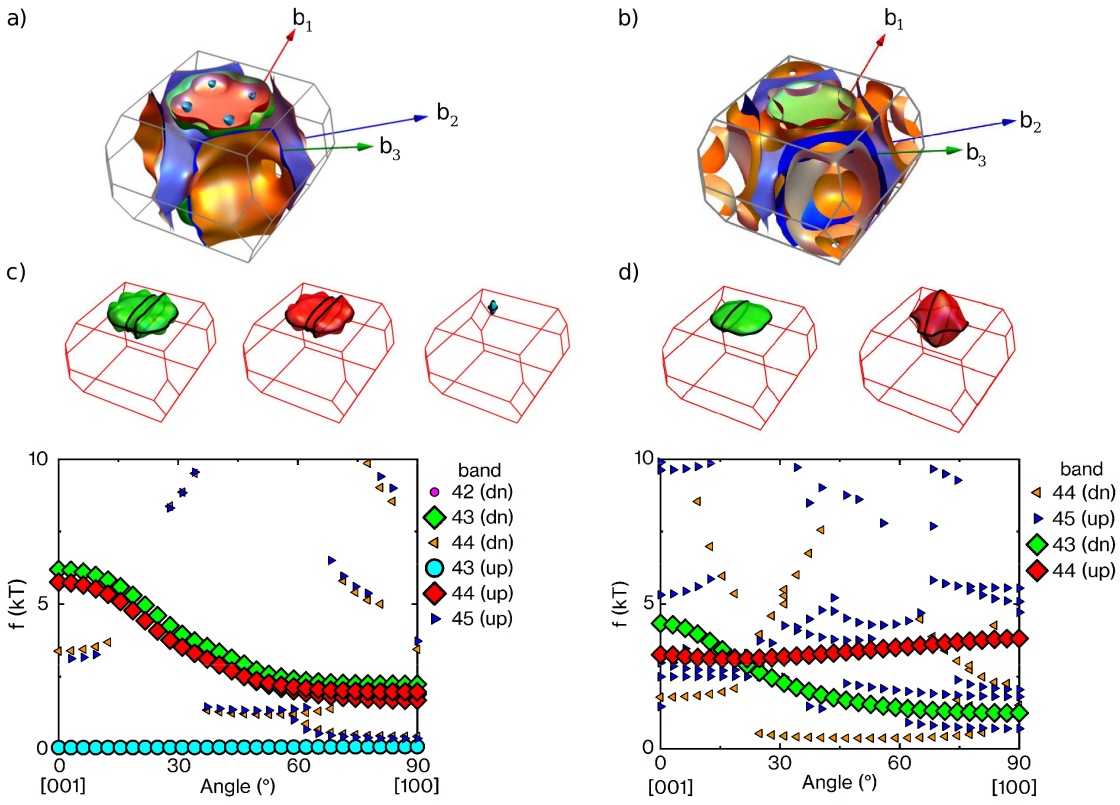

Figure 3: Fermi surfaces and dHvA spectrum of $CeAuAl_3$: a) Fermi surface for a localized 4f-electron comprising of 6 sheets (LDA+U+SOC with U=4 eV). Sheet 6 is hardly visible due to its small size. b) Fermi surface for an itinerant 4f-electron comprising of 4 sheets (LDA). c) dHvA spectrum and characteristic orbits for a localized 4f-electron (LDA+U with U=4 eV). d) dHvA spectrum and characteristic orbits for an itinerant 4f-electron (LDA). The labeling of the Fermi surface sheets and orbits is shown in the legends of panels c) and d). The same colors are used for the same bands, e.g., band 44 (up) for the localized 4f-electron is colored in red as is band 44 (up) for the itinerant 4f-electron.

The Fermi surface of the localized 4f-electron consists of 6 sheets which show a distinctly different Fermi surface topology as compared to itinerant 4f-electrons with 4 sheets (figures 3a) and 3b)). Calculating the dHvA orbits for both cases makes their differences apparent. This is shown in figures 3c) and 3d) where we show three selected orbits for localized f-electrons and 2 selected orbits for itinerant f-electrons, respectively. For this figure we chose the orbits shown because they may be traced for all magnetic field directions between [100] and [001]. The Fermi surface sheet marked in cyan (band 43 (up)) of the localized 4f-electron vanishes for itinerant 4f-electrons. Thus, no flat dispersing orbit at very low frequencies is observed in the dHvA spectrum of the itinerant 4f-electrons. For the sheet marked in green (band 43 (dn)) the dispersion remains similar but the size of the orbits is reduced. The sheet marked in red (band 44 (up)) completely changes its shape and hence the dispersion of the orbit. Furthermore, the orange (band 44 (dn)) and blue (band 45 (up)) sheets grow in size and are more complex when going from the localized to the itinerant configuration. In turn, we expect additional frequencies in the dHvA spectra of itinerant 4f-electrons. To summarize, we observe distinct features of the Fermi surface and the dHvA spectra unique to the localized or itinerant f-electrons. It is finally possible to comment the small Fermi surface of the localized 4f-electron and the large Fermi surface of the itinerant 4f-electron to different parts of the magnetic phase diagram. From the experimental findings on the specific heat and inelastic neutron scattering we would expect a small Fermi surface at high temperatures as well as low temperatures above moderate magnetic fields. In comparison, the properties of itinerant f-electrons according to the specific heat data should be observable below 4 K for magnetic fields up to a few Tesla.

4 Conclusions

We calculated the structural and magnetic properties of $CeAuAl_3$ using density functional theory. Assuming a localized 4f-electron picture by using DFT+U, our results are in good agreement with experiment. We also present predictions of the electronic structure and Fermi surfaces for a localized and an itinerant 4f-electron. We predict that the two cases may be readily distinguished in quantum oscillation measurements. In addition we consider where to expect a small and large Fermi surface in the magnetic phase diagram.

Acknowledgements

We wish to thank A. Bauer, P. Cermak, D. Eckert, C. Franz, A. Schneidewind, and M. Stekiel for discussions.

Funding information We gratefully acknowledge financial support by the DFG in the framework of TRR80 (project id 107745057), SPP 2137 (Skyrmionics) under grant no. PF393/19 (project id 403191981), DFG-GACR project WI 3320/3-1, ERC Advanced grant 788031 (ExQuiSid), and Germany's excellence strategy EXC-2111 390814868.

A Computational Details

The exchange correlation functionals used in our calculations are LDA [23], PBE [24] and PBEsol [25]. The muffin tin radii R_{MT} were set to 2.21 b for Ce, 2.30 b for Au and 2.00 b for Al and RK_M was set to 9.5 in WIEN2k and 9.0 in Elk. The results are well converged for $RK_M \geq 9.0$. The cut off energy between valence and core electrons is −8.3 Ry. Different k-grids

were used for specific physical properties. In WIEN2k and Elk different symmetry settings are used for the unit cells and their k-grids. Therefore, we specifically report the unit cell and the DFT package for each k-grid. Structure optimization was done with a 21x21x21 grid (primitive cell, WIEN2k), the electronic and magnetic properties with a 36x36x36 grid (primitive cell, WIEN2k) and the helical magnetic structure with a 18x18x7 grid (conventional unit cell, Elk).

References

[1] S. Paschen, E. Felder and H. Ott, *Transport and thermodynamic properties of $CeAuAl_3$*, The European Physical Journal B **2**, 169 (1998), doi:10.1007/s100510050237.

[2] D. T. Adroja, C. de la Fuente, A. Fraile, A. D. Hillier, A. Daoud-Aladine, W. Kockelmann, J. W. Taylor, M. M. Koza, E. Burzurí, F. Luis, J. I. Arnaudas and A. del Moral, *Muon spin rotation and neutron scattering study of the noncentrosymmetric tetragonal compound $CeAuAl_3$*, Physical Review B **91**, 134425 (2015), doi:10.1103/PhysRevB.91.134425.

[3] M. Stekiel, P. Cermak, M. Meven, C. Franz, S. Weber, R. Schoenmann, V. Kumar, K. Nemkovskiy, H. Deng, A. Bauer, C. Pfleiderer and A. Schneidewind, *Magnetic ordering in non-centrosymmetric $CePdAl_3$ and $CePtAl_3$* (2021).

[4] D. T. Adroja, A. del Moral, C. de la Fuente, A. Fraile, E. A. Goremychkin, J. W. Taylor, A. D. Hillier and F. Fernandez-Alonso, *Vibron quasibound state in the noncentrosymmetric tetragonal heavy-fermion compound $CeCuAl_3$*, Physical Review Letters **108**, 216402 (2012), doi:10.1103/PhysRevLett.108.216402.

[5] P. Čermák, A. Schneidewind, B. Liu, M. M. Koza, C. Franz, R. Schönmann, O. Sobolev and C. Pfleiderer, *Magnetoelastic hybrid excitations in $CeAuAl_3$*, Proceedings of the National Academy of Sciences **116**, 6695 (2019), doi:10.1073/pnas.1819664116.

[6] J. M. Luttinger, *Fermi surface and some simple equilibrium properties of a system of interacting fermions*, Physical Review **119**, 1153 (1960), doi:10.1103/PhysRev.119.1153.

[7] R. M. Martin, *Fermi-surfae sum rule and its consequences for periodic kondo and mixed-valence systems*, Physical Review Letters **48**, 362 (1982), doi:10.1103/PhysRevLett.48.362.

[8] H. Shishido, R. Settai, H. Harima and Y. Ōnuki, *A drastic change of the fermi surface at a critical pressure in $CeRhIn_5$: dhva study under pressure*, Journal of the Physical Society of Japan **74**, 1103 (2005), doi:10.1143/JPSJ.74.1103.

[9] H. Aoki, S. Uji, A. K. Albessard and Y. Ōnuki, *Transition of f-electron nature from itinerant to localized: Metamagnetic transition in $CeRu_2Si_2$ studied via the de haas–van alphen effect*, Physical Review Letters **71**, 2110 (1993), doi:10.1103/PhysRevLett.71.2110.

[10] J. H. Shim, K. Haule and G. Kotliar, *Modeling the localized-to-itinerant electronic transition in the heavy fermion system $CeIrIn_5$*, Science **318**, 1615 (2007), doi:10.1126/science.1149064.

[11] P. Blaha, K. Schwarz, F. Tran, R. Laskowski, G. K. H. Madsen and L. D. Marks, *Wien2k: An apw+lo program for calculating the properties of solids*, The Journal of Chemical Physics **152**, 074101 (2020), doi:10.1063/1.5143061.

[12] *The Elk code, https://elk.sourceforge.io/*.

[13] L. M. Sandratskii, *Symmetry analysis of electronic states for crystals with spiral magnetic order. i. general properties*, Journal of Physics: Condensed Matter **3**, 8565 (1991), doi:10.1088/0953-8984/3/44/004.

[14] A. I. Liechtenstein, V. I. Anisimov and J. Zaanen, *Density-functional theory and strong interactions: Orbital ordering in mott-hubbard insulators*, Physical Review B **52**, R5467 (1995), doi:10.1103/PhysRevB.52.R5467.

[15] A. Shick, W. Pickett and A. Liechtenstein, *Ground and metastable states in $\gamma - Ce$ from correlated band theory*, Journal of Electron Spectroscopy and Related Phenomena **114-116**, 753 (2001), doi:10.1016/S0368-2048(00)00394-7.

[16] C. Franz, A. Senyshyn, A. Regnat, C. Duvinage, R. Schönmann, A. Bauer, Y. Prots, L. Akselrud, V. Hlukhyy, V. Baran and C. Pfleiderer, *Single crystal growth of $CeTAl_3$ $(T = Cu, Ag, Au, Pd and Pt)$*, Journal of Alloys and Compounds **688**, 978 (2016), doi:10.1016/j.jallcom.2016.07.071.

[17] H. Sugawara, S. Saha, T. Matsuda, Y. Aoki, H. Sato, J. Gavilano and H. Ott, *Magnetic and transport properties in $CeAuAl_3$ single crystal*, Physica B: Condensed Matter **259-261**, 16 (1999), doi:10.1016/S0921-4526(98)00814-X.

[18] C. Franz, *Untersuchung von $Quantenphasenbergngen$ bei fehlender $Inversionssymmetrie$* (2014).

[19] T. Jarlborg, A. Freeman and D. Koelling, *The electronic structure and properties of the c15 compounds $CeAl_2$, $LaAl_2$ and YAl_2*, Journal of Magnetism and Magnetic Materials **60**, 291 (1986), doi:10.1016/0304-8853(86)90113-7.

[20] F. Tran, F. Karsai and P. Blaha, *Nonmagnetic and ferromagnetic fcc cerium studied with one-electron methods*, Physical Review B **89**, 155106 (2014), doi:10.1103/PhysRevB.89.155106.

[21] G. Zwicknagl, *Quasi-particles in heavy fermion systems*, Advances in Physics **41**, 203 (1992), doi:10.1080/00018739200101503.

[22] G. Zwicknagl, *The utility of band theory in strongly correlated electron systems*, Reports on Progress in Physics **79**(12), 124501 (2016), doi:10.1088/0034-4885/79/12/124501.

[23] J. P. Perdew and Y. Wang, *Accurate and simple analytic representation of the electron-gas correlation energy*, Phys. Rev. B **45**, 13244 (1992), doi:10.1103/PhysRevB.45.13244.

[24] J. P. Perdew, K. Burke and M. Ernzerhof, *Generalized gradient approximation made simple*, Phys. Rev. Lett. **77**, 3865 (1996), doi:10.1103/PhysRevLett.77.3865.

[25] J. P. Perdew, A. Ruzsinszky, G. I. Csonka, O. A. Vydrov, G. E. Scuseria, L. A. Constantin, X. Zhou and K. Burke, *Restoring the density-gradient expansion for exchange in solids and surfaces*, Phys. Rev. Lett. **100**, 136406 (2008), doi:10.1103/PhysRevLett.100.136406.